Nonlinear Dyn (2020) 100:2657–2672
https://doi.org/10.1007/s11071-020-05593-8

ORIGINAL PAPER

Energy-efficient firing patterns with sparse bursts in the Chay neuron model

Fengyun Zhu · Rubin Wang · Kazuyuki Aihara · Xiaochuan Pan

Received: 12 December 2019 / Accepted: 22 March 2020 / Published online: 18 April 2020
© Springer Nature B.V. 2020

Abstract The energy efficiency of neural signal transmission is thought to be an important constraint in the nervous system. It is generally measured as the energy consumed per unit of information. Most of the previous studies have demonstrated this efficiency by focusing on single action potentials. However, neural information is more likely to be encoded by a spike train rather than by a single spike. To date, how the energy efficiency is dependent on patterns of spike trains is still unclear. In this study, we examined the energy efficiency of various firing patterns simulated by the Chay neuron model, including relatively high-frequency activities with massive spikes, medium-frequency activities with a moderate number of spikes, and low-frequency activities with rare spikes. Our results indicate that medium-frequency patterns are more energy efficient than both the high-frequency and low-frequency patterns. The most efficient medium-frequency pattern is a sparse burst firing (SBF) pattern because it consumes minimal energy and transmits an amount of neural information comparable to that of high-frequency patterns which consume much more energy. SBF patterns minimize energy consumption not only by producing fewer spikes than high-frequency patterns, but more importantly, also by consuming available energy sources, namely the potential energy stored in ionic concentration gradients, in a balanced way. Furthermore, with fewer spikes, the irregular spike trains of SBF patterns with short bursts and single spikes maximize the neural information that they carry, leading to higher energy efficiency. Thus, the sensory system may give priority to limiting energy costs over maximizing information to achieve greater energy efficiency.

Keywords Sparse burst firing · Chay neuron model · Neural energy consumption · Coefficient of variation · Na/K-ATPase pump

F. Zhu · R. Wang (✉) · X. Pan (✉)
Institute for Cognitive Neurodynamics, School of Science, East China University of Science and Technology, Shanghai 200237, China
e-mail: rbwang@163.com
e-mail: pxc@ecust.edu.cn

F. Zhu · K. Aihara
Institute of Industrial Science, The University of Tokyo, Tokyo 153-8505, Japan

1 Introduction

Neurons in many sensory systems generate action potentials (APs or spikes) in distinct temporal patterns to transmit information to connected neurons. Sparse burst firing (SBF), a combination of single spikes and much less numerous short bursts of 2–8 spikes, is one of the most common patterns observed in visual, auditory, and motor sensory systems [1–6]. High-frequency firing and low-frequency tonic firing patterns also occur in sensory information processing [7–10]. Neuronal coding theory hypothesizes that information is coded in the structure of the spike

train of these firing patterns [11–15]. Generating these information-carrying action potential sequences consumes considerable energy [16–18]. In this process, ionic concentration gradients of Na^+ and K^+ are partially dissipated and must be restored and maintained with Na/K-ATPase pumps by hydrolyzing adenosine triphosphate (ATP) [16,19].

Sensory information processing is thought to have evolved within a restricted energy budget, resulting in a trend toward energy efficiency [20–23]. Energy efficiency can be measured as the energy consumed per unit of transmitted information [23,24]. Most of the previous theoretical and experimental studies have demonstrated this efficiency by focusing on how the underlying ionic currents, such as Na^+ and K^+ currents, influence the energy efficiency of single APs of different neurons [19,21,22]. For instance, Alle et al. [21] showed that in rat hippocampus mossy fiber axons, the smaller temporal overlap of the inward Na^+ current and the outward K^+ current during APs leads to fewer energy costs and greater energy efficiency, assuming that each AP transmits equivalent information. However, the energy efficiency of a neuron depends not only on its single APs but also on its firing pattern. In fact, some essential properties of the firing pattern, such as the firing frequency, the firing modes (i.e., single spikes and bursts), the shape of spikes, and the extent of hyperpolarization after spikes, significantly affect energy consumption and/or information transmission [10,22], and thus the energy efficiency. These properties are mainly modulated by underlying K^+ currents, including calcium-dependent K^+ currents and voltage-dependent K^+ currents [10,22,25–27]. For example, Goldberg et al. [10] demonstrated that the reduction of a specific calcium-dependent K^+ current can generate a transition from irregular low-frequency single spiking to rhythmic high-frequency bursting with distinct hyperpolarization, and Carter et al. [22] showed that the width of APs is mainly determined by the K^+ channels in nerve membranes. In auditory brainstem neurons, the voltage-dependent K^+ channels responsible for repolarization are also known to influence their firing modes [25]. However, how the underlying K^+ currents affect all these properties of a firing pattern to promote energy efficiency remains unclear. In other words, since a neuron can fire in different firing patterns by modulating the K^+ currents, a particular firing pattern may be more energy efficient than others. Exploring this hypothesis is essential for a better understanding of the mechanisms underlying information encoding [28–31] in the nervous system.

In this study, we modified the K^+ currents in the Chay neuron model [32] to simulate diverse firing patterns similar to those observed in electrophysiological experiments [10] and assessed the energy efficiency of these patterns. Our findings indicate that medium-frequency firing patterns consume roughly as little energy as low-frequency patterns do, but can carry nearly as much information as high-frequency patterns that consume much more energy, suggesting that medium-frequency firing patterns are more energy efficient than other patterns. Specifically, the most efficient pattern is a medium-frequency SBF, which minimizes energy costs by consuming energy sources (the potential energy stored in ionic concentration gradients) in a balanced way, and maximizes neural information by producing more informative spikes with the combination of short bursts and single spikes. This study suggests that the prevalence of these SBF patterns is an important way for the sensory system to achieve energy efficiency in information transmission.

2 Model and method

2.1 The Chay model and different firing properties

The Chay neuron model [32] provides a simple and effective tool to simulate different firing patterns in the biological nervous system with comprehensive dynamical analyses [33–35]. The model is described as follows:

$$\mathrm{d}V/\mathrm{d}t = -I_i - I_{\mathrm{kv}} - I_{\mathrm{kc}} - I_l, \tag{1}$$

$$\mathrm{d}n/\mathrm{d}t = (n_\infty\text{-}n)\big/\tau_n, \tag{2}$$

$$\mathrm{d}C/\mathrm{d}t = \rho\left(m_\infty^3 h_\infty (V_c - V) - k_c C\right), \tag{3}$$

where V, n, and C are the membrane potential, the probability of opening voltage-dependent K^+ channels, and the intracellular Ca^{2+} concentration, respectively. In Eq. (1), I_i is the inward mixed Na^+–Ca^{2+} ionic current; I_{kv} is the outward voltage-dependent K^+ ionic current; I_{kc} is the outward calcium-dependent K^+ ionic current; I_l is the leakage current. I_i, I_{kv}, I_{kc}, and I_l are described as follows:

$$I_i = g_i m_\infty^3 h_\infty (V - V_i), \tag{4}$$

$$I_{\mathrm{kv}} = g_{\mathrm{kv}} n^4 (V - V_k), \tag{5}$$

$$I_{kc} = g_{kc}(C/(1+C))(V - V_k), \quad (6)$$

$$I_l = g_l\,(V - V_l)\,, \quad (7)$$

where V_i, V_k, and V_l are the reversal potentials for mixed Na^+–Ca^{2+}, K^+, and leakage ions, respectively; g_i, g_{kv}, g_{kc}, and g_l represent the maximal conductances, where the subscripts (i), (kv), (kc), and (l) refer to the voltage-dependent mixed ionic channel, the voltage-dependent K^+ channel, the Ca^{2+}-dependent K^+ channel, and leakage channels, respectively. m_∞ and h_∞ in Eq. (4) are the probabilities of activation and inactivation of the mixed channel, respectively; n_∞ in Eq. (2) is the steady-state value of n. They are expressed as follows: $y_\infty = \alpha_y(V)/(\alpha_y(V) + \beta_y(V))$, $y = m$, h, or n, with nonlinear functions $\alpha_y(V)$ and $\beta_y(V)$ given by

$$\alpha_m\,(V) = 0.1(25+V)/(1-e^{-0.1V-2.5}), \quad (8)$$

$$\beta_m\,(V) = 4e^{-(V+50)/18}, \quad (9)$$

$$\alpha_h\,(V) = 0.07e^{-0.05V-2.5}, \quad (10)$$

$$\beta_h\,(V) = 1/(1+e^{-0.1V-2}), \quad (11)$$

$$\alpha_n\,(V) = 0.01(20+V)/(1-e^{-0.1V-2}), \quad (12)$$

$$\beta_n\,(V) = 0.125e^{-(V+30)/80}, \quad (13)$$

In Eq. (2), the relaxation time of the voltage-dependent K^+ channel (τ_n) is described as follows:

$$\tau_n = 1/(\lambda_n(\alpha_n + \beta_n)), \quad (14)$$

where λ_n, a scaling term of the relaxation time constant, controls the shapes of APs as well as the extent of hyperpolarization. In Eq. (3), k_c is the rate constant for the efflux of the intracellular Ca^{2+}, ρ is a proportionality constant, and V_c is the reversal potential for Ca^{2+} ions. The values of the reversal potentials and the fixed parameters used in this study are listed in Table 1.

Table 1 Parameter values used in the numerical simulations

Parameter	Value	Unit
V_i	100	mV
V_k	−75	mV
V_l	−40	mV
V_c	100	mV
g_i	1800	μS
g_{kv}	1700	μS
g_l	7	μS
ρ	0.27	
k_c	3.3/18	

In the Chay model, K^+ currents, including the calcium-dependent K^+ current I_{kc} in Eq. (6) and the voltage-dependent K^+ current I_{kv} in Eq. (5), significantly influence the dynamics of the system. Modifying the maximal conductance g_{kc} of I_{kc} in Eq. (6) causes the neuron model to discharge in different firing patterns, from burst firing with different burst sizes to tonic firing and irregular chaotic firing [32]; for a detailed bifurcation analysis of g_{kc}, please refer to [32]. Modifying the scaling term λ_n for the relaxation time constant of voltage-dependent K^+ channels in Eq. (14) generates changes in APs with different extents of hyperpolarization and reshapes the firing pattern [33]. In contrast, modifying the maximal conductance of voltage-dependent K^+ channels g_{kv} or the maximal conductance of Na^+–Ca^{2+} mixed ionic channels g_i, whose dynamic functions in the Chay model are to determine the peak amplitude of the AP or to produce stereotyped burst modes, results in little significant change in firing patterns, especially the spike-timing patterns. In other words, in the Chay model, g_{kc} mainly controls the firing frequency as well as the firing modes, and the value of λ_n determines the width of spikes and the degree of hyperpolarization of firing patterns. Therefore, in this study, we examined the energy efficiency of firing patterns generated by the changes of g_{kc} and λ_n while keeping g_{kv} and g_i constant. All firing patterns were simulated with identical initial conditions of $V\,(0) = -48.25$ mV, $n\,(0) = 0.20$, and $C\,(0) = 0.40$.

Figure 1 shows some representative examples of single spikes, bursts, and hyperpolarization in different firing patterns simulated by modifying the K^+ currents in the Chay model. Bursts are defined as a set of spikes whose interspike intervals (ISI) are shorter than .52 s according to the firing characteristics of the Chay model neuron and its timescale [2,32]. The burst size N_b of a firing pattern is calculated as the average number of spikes per burst. In sensory systems, a firing pattern is called SBF if its burst size satisfies $2 \leqslant N_b \leqslant 8$ and its burst probability is in the range of 1–35% [4–6]. One spike preceded and followed by a time interval greater than 0.52 s is called a single spike, and N_s is the total number of single spikes in a firing pattern. The width and amplitude of spikes may differ from one firing pattern to another (Fig. 1b–e). Hyperpolarization after spikes also exhibits different durations and intensities in different firing patterns (Fig. 1b–e). These diverse firing properties have been observed in different neurons in electrophysiological experiments when phar-

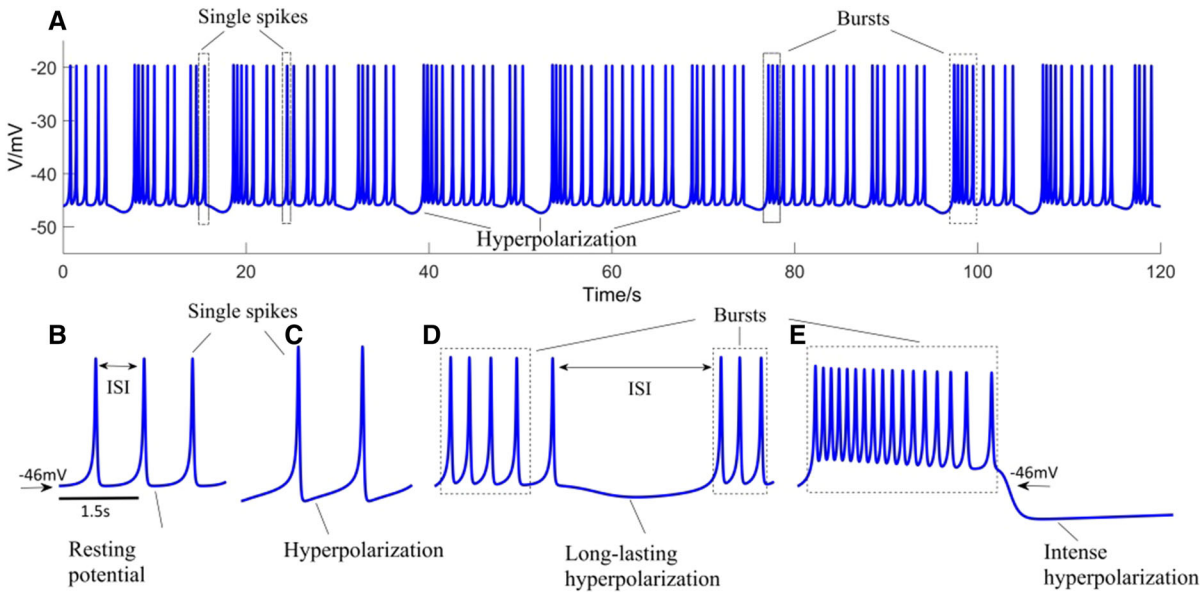

Fig. 1 Examples of various single spikes, bursts, and hyperpolarization simulated with different values of g_{kc} and λ_n in the Chay model. **a** A chaotic firing pattern in which single spikes and bursts are interrupted by hyperpolarization of different degrees, simulated with $g_{kc} = 11\,\mu S$ and $\lambda_n = 230$. **b** Single spikes with the membrane returning to resting potential without hyperpolarization, enlarged from a firing pattern with $g_{kc} = 10\,\mu S$ and $\lambda_n = 230$. **c** Singe spikes with larger width and amplitude followed by a short phase of hyperpolarization, enlarged from a firing pattern with $g_{kc} = 11.5\,\mu S$ and $\lambda_n = 180$. **d** A burst proceeded by slow, long-lasting hyperpolarization, enlarged from a firing pattern with $g_{kc} = 11.5\,\mu S$ and $\lambda_n = 230$. **e** A burst followed by intense hyperpolarization, enlarged from a firing pattern with $g_{kc} = 13\,\mu S$ and $\lambda_n = 280$. In the Chay model, hyperpolarization is characterized by the membrane potential repolarizing below the threshold potential of -46 mV

macologically manipulating calcium-dependent and/or voltage-dependent K^+ channels [10,25,27].

It should be noted that the firing frequency is very low in the Chay model compared with real biological systems because of the time scale used. Nevertheless, the Chay model is very effective in simulating the essential properties of distinctive firing patterns, including the number and frequency of spikes, burst and single spike modes, shapes of spikes, and extent of hyperpolarization. Therefore, the firing frequencies used in this study are relative to those frequencies that the Chay model can generate.

2.2 Estimation of energy consumption

Previous experimental studies suggest that the extensive overlap of inward Na^+ currents and outward K^+ currents during APs wastes Na^+ and K^+ and accordingly wastes energy [19,21]. This wasted energy does not contribute to the change of membrane potential and the transmission of information. Therefore, we estimated only the energy effectively used to generate neuronal signals, i.e., membrane voltage changes during a firing pattern. To do so, we used the energy estimation method proposed in our previous studies [36,37], which is based on the equivalent circuit of the Chay model [38], as shown in Fig. 2a. As do most neural models, the Chay model has a default assumption that reversal potentials are supported by Na/K-ATPase pumps by consuming ATP to create and maintain the concentration gradients of ions across the membrane [38]. In other words, the electrical potential energy stored in the reversal potentials V_y $(y = i, k, l)$, i.e., the batteries in the circuit, is ultimately derived from the biological energy ATP consumed by Na/K-ATPase pumps.

These batteries provide currents I_y $(y = i, k, l)$ to change the voltage across the capacitor C_m, and neuronal activity is generated accordingly. The rate of electrical energy (power) transferred to the capacitor by each battery is its electrical current multiplied by its electromotive force, i.e., $|I_y V_y|(y = i, k, l)$

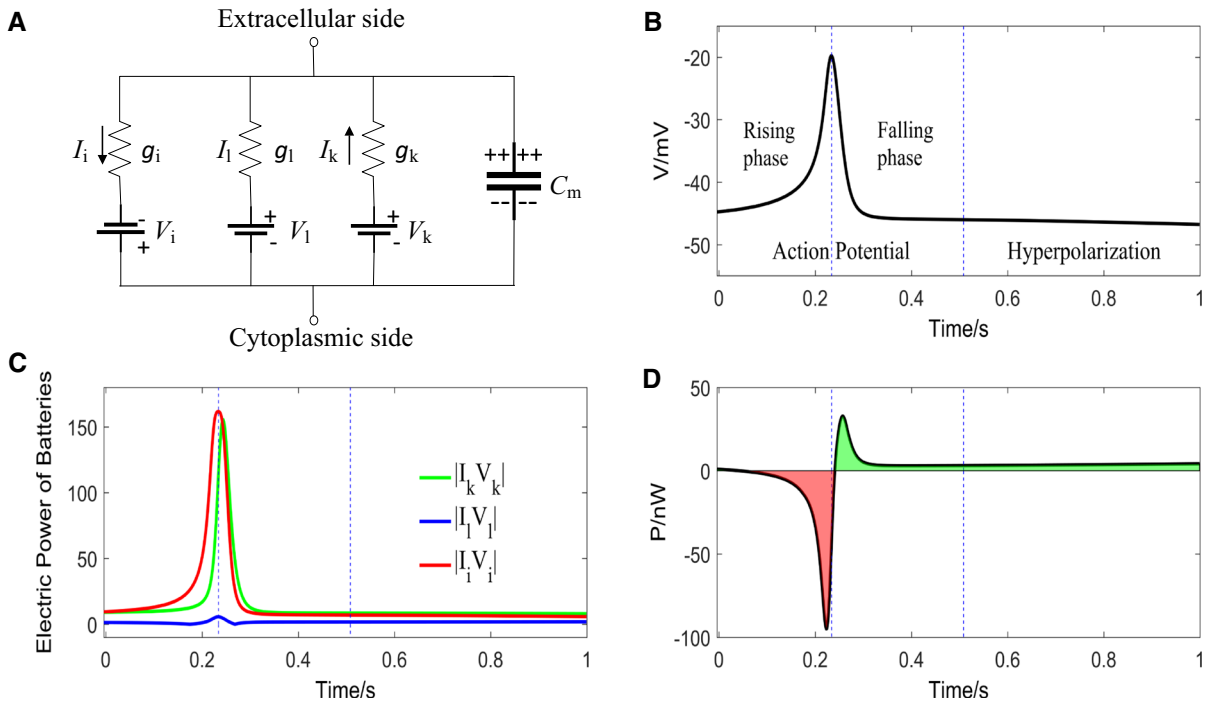

Fig. 2 The net power P of membrane potential changes during an AP and its following hyperpolarization. **a** The equivalent circuit of the Chay neuron model with three batteries providing charges to the capacitor C_m (i.e., membrane voltage). I_k represents the sum of the K^+ currents I_{kv} and I_{kc} in the Chay model. The other two currents (mixed Na^+–Ca^{2+} current I_i and leakage current I_l) and the reversal potentials V_y $(y = i, k, l)$ are the same as in the model. **b** An AP with its rising and falling phases, as well as its following hyperpolarization, is divided by the blue dashed lines. **c** Corresponding electric power provided by three batteries to the capacitor. During the rising phase, the electric power $|I_iV_i|$ (the red line) provided by battery V_i is mostly bigger than the electric power $|I_kV_k| + |I_lV_l|$ (the green and blue lines) provided by batteries V_k and V_l to depolarize the membrane. During the falling phase and hyperpolarization, the latter is bigger than the former to repolarize and further hyperpolarize the membrane. **d** The corresponding net power P during the AP and its following hyperpolarization. When P is negative, the energy consumed to change the membrane potential comes from the net electric power of $|I_iV_i|$, which is not counterbalanced by the electric power of $|I_kV_k| + |I_lV_l|$. Conversely, when P is positive, the energy consumed to change the membrane potential comes from the net electric power of $|I_kV_k| + |I_lV_l|$, which is not counterbalanced by the electric power of $|I_iV_i|$. (Color figure online)

[36,37,39–41], as shown in Fig. 2c. Thus, the rate of energy change of the potential difference across the membrane should be the sum of the electric power provided by each battery. However, the electric power provided by each battery has different effects on the transmembrane potential. The electric power provided by battery V_i makes the membrane potential less negative (depolarization), while the electric power provided by batteries V_k and V_l generally makes the membrane potential more negative (repolarization). Consequently, the net power P that contributes to membrane voltage changes in the Chay model is estimated as follows:

$$P(t) = |I_k * V_k| + |I_l * V_l| - |I_i * V_i| . \quad (15)$$

where I_k is the sum of the K^+ currents I_{kv} and I_{kc}. (Note that, in the Chay model, whether or not each power is calculated in absolute value terms has no significant effect on the results, because I_yV_y $(y = i, k, l)$ is almost always negative.) Thus, depending on which of the voltage sources (V_k, V_l) or (V_i) provides more electric power, the value of the net power P in Eq. (15) can be positive or negative. As shown in Fig. 2b, d, during the rising phase of an AP, the net power P is negative, immediately turns positive during the falling phase, and remains positive during hyperpolarization.

We define the negative energy that is consumed during a time period T of a firing pattern when P is negative using the following equation:

$$E_{negative} = \begin{cases} \int_0^T -P(t)\mathrm{d}t, & P < 0 \\ 0, & P \geq 0 \end{cases}. \quad (16)$$

Conversely, when P is positive, the positive energy consumed during the time period T is defined as

$$E_{positive} = \begin{cases} 0, & P < 0 \\ \int_0^T P(t)\,\mathrm{d}t, & P \geq 0 \end{cases}. \quad (17)$$

Therefore, the neural energy consumption E contributing to the membrane potential changes during the firing activity is defined as

$$E = E_{negative} + E_{positive} = \int_0^T |P(t)|\mathrm{d}t. \quad (18)$$

We set $T = 30$ s in the following simulation. In Sect. 3.2, we will vary T from 5 to 60 s to examine the relationship between time and energy efficiency. As shown in Fig. 2d, APs consume both negative energy (the red area) and positive energy (the green area), and the former is usually greater than the latter. Hyperpolarization, by contrast, consumes only positive energy (the green area), as does the resting potential.

For the sake of mathematical convenience, we assume the ratio of the consumption of negative energy to the consumption of positive energy to be δ, which is defined as

$$\delta = E_{negative} / E_{positive}. \quad (19)$$

Hereafter, we call it the $E_n - E_p$ ratio. Thus, if a firing pattern fires only APs without hyperpolarization, the $E_n - E_p$ ratio will be much bigger than 1; if the firing pattern is so hyperpolarized as to limit firing activity to very few or no AP, this ratio will be closer to 0.

2.3 Information representation and energy efficiency

The amount of information carried by a firing pattern is usually defined in Shannon's terms as the relation of neural response to a given stimulus [12,42,43]. In this study, however, the firing patterns were simulated by changing the conductance of ionic channels of the Chay model in the absence of a stimulus. While it is still under debate about how neural information is coded, one popular hypothesis is that the precise timing of each spike is significant, and the temporal variability of a spike train provides a large capacity for carrying information [44,45]. We adopt this hypothesis in this study and thus use the variability of the spike train itself, i.e., its coefficient of variability (CV) [46,47], to represent the amount of carried information.

Each firing pattern in this study is converted into a sequence of ISIs $\{t_1, t_2, t_3, \ldots, t_N\}$ with a mean μ and a standard deviation σ given by

$$\mu = \frac{1}{N}\sum_{n=1}^{N} t_n, \quad \sigma = \sqrt{\frac{1}{N}\sum_{n=1}^{N}(t_n - \mu)^2}. \quad (20)$$

Then, the coefficient of variation (CV) of the spike train variability is given as

$$\mathrm{CV} = \sigma/\mu. \quad (21)$$

According to this definition and the above neural coding hypothesis [44,45], the more irregular the firing pattern is, the larger the value of CV is and accordingly the more information it carries.

We then examine the energy efficiency of a firing pattern by measuring the energy consumption per unit of information given as

$$\eta = E/\mathrm{CV}. \quad (22)$$

The smaller the value of η is, the lower the energy consumption per unit of information is (i.e., the greater the energy efficiency). Conversely, a higher η value signifies less energy efficiency.

3 Results

3.1 Energy efficiency of firing patterns resulting from changing the maximal conductance of the Ca^{2+}-dependent K^+ channel g_{kc}

We first examined the energy efficiency of firing patterns resulting from modifying the parameter g_{kc} in Eq. (6). We varied g_{kc} from 6 to 23.6 μS in steps of 0.2 in generating firing patterns with the Chay model and determined the burst size N_b (the red points in Fig. 3a), the number of single spikes N_s (the green points in Fig. 3a), the total number of spikes N (Fig. 3b), and the probability of bursts (Fig. 3c) for each firing pattern. These firing patterns can be broadly divided into the following three categories: 1) High-frequency patterns with massive spikes (g_{kc}: 6–9). The neuron discharges a large number of spikes (N: 61–135 spikes, Fig. 3b), and these spikes come either in a very large high-frequency burst (most $N_b > 29$) or in single spike modes (Fig. 3a). 2) Medium-frequency patterns with fewer spikes (g_{kc}: 9.2–12). The neuron fires in both burst and single spike modes with a moderate total number of spikes (N: 24–57 spikes, the colored bars

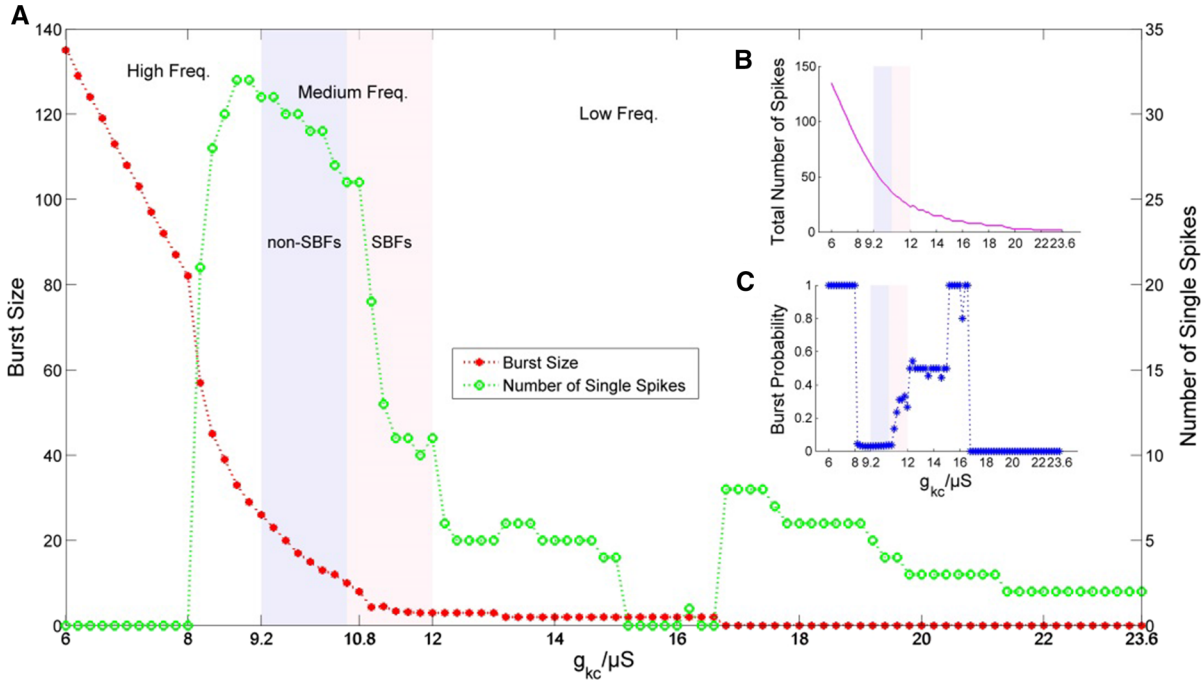

Fig. 3 Characteristics of various firing patterns resulting from changing the maximal conductance of the Ca^{2+}-dependent K^+ channel g_{kc} from 6 to 23.6 μS in the Chay model. **a** Burst sizes, i.e., the average number of spikes per burst (the red points) and the number of single spikes (the green points). **b** The total number of spikes N as a function of g_{kc} (the violet line). **c** The probability of bursts (the blue points), i.e., the ratio of the number of bursts to the total number of bursts and single spikes in each firing pattern. All three figures are divided into three regions: high-frequency patterns (g_{kc}: 6–9), medium-frequency patterns (g_{kc}: 9.2–12), and low-frequency patterns (g_{kc}: 12.2–23.6). Within the medium-frequency category, we can further distinguish sparse burst firing patterns (SBFs, the pink column) from other patterns (non-SBFs, the light-blue column). All these firing patterns are simulated with a fixed λ_n of 230. (Color figure online)

in Fig. 3b), a gradually decreasing burst size N_b (the colored bars in Fig. 3a), and a rising trend in burst probability (the colored bars in Fig. 3c). In particular, when g_{kc} rises from 10.8 to 12, the firing pattern shifts to SBFs (the pink-colored bar in Fig. 3), whose burst size satisfies $2 \leqslant N_b \leqslant 8$ and burst probability is in the range of 1–35% [4–6]. For example, a g_{kc} of 10.8 generates an SBF with $N_b = 8$ spikes, $N_s = 26$ spikes, and a burst probability of about 4%. 3) Low-frequency patterns with rare spikes (g_{kc}: 12.2–23.6). The total number of spikes discharged by the neuron is small (N: 1–23 spikes). Some of these firing patterns do contain bursts and single spikes, but their mode is nearly identical in contrast to SBFs. When $g_{kc} \geq 16.8$, only a few single spikes appear. The above frequency division is mapped from the most commonly used division of frequencies in the nervous system: a high-frequency gamma range of 30–80 Hz, a medium-frequency beta range of 13–30 Hz, and a low-frequency delta/theta/alpha range of 0.5–12 Hz [48,49]. Small shifts in the boundaries of these divisions have no effect on the results of this study.

Three typical firing patterns were selected from each category to examine their positive and negative energy consumption properties, as shown in Fig. 4. At a small value of $g_{kc} = 6$ (the blue line), spikes are emitted in a very intensive and phasic firing pattern without hyperpolarization because the small calcium-dependent current I_{kc} is too weak to hyperpolarize the membrane potential. The membrane potential of this high-frequency pattern is almost always above the threshold potential of −46 mV (the red dashed line, Fig. 4b). This pattern consumes three times more negative energy than positive energy (Fig. 4e) because discharging APs alone without hyperpolarization consumes more negative energy than positive energy (Fig. 2d). A g_{kc} of 11.4 (the black line) produces a

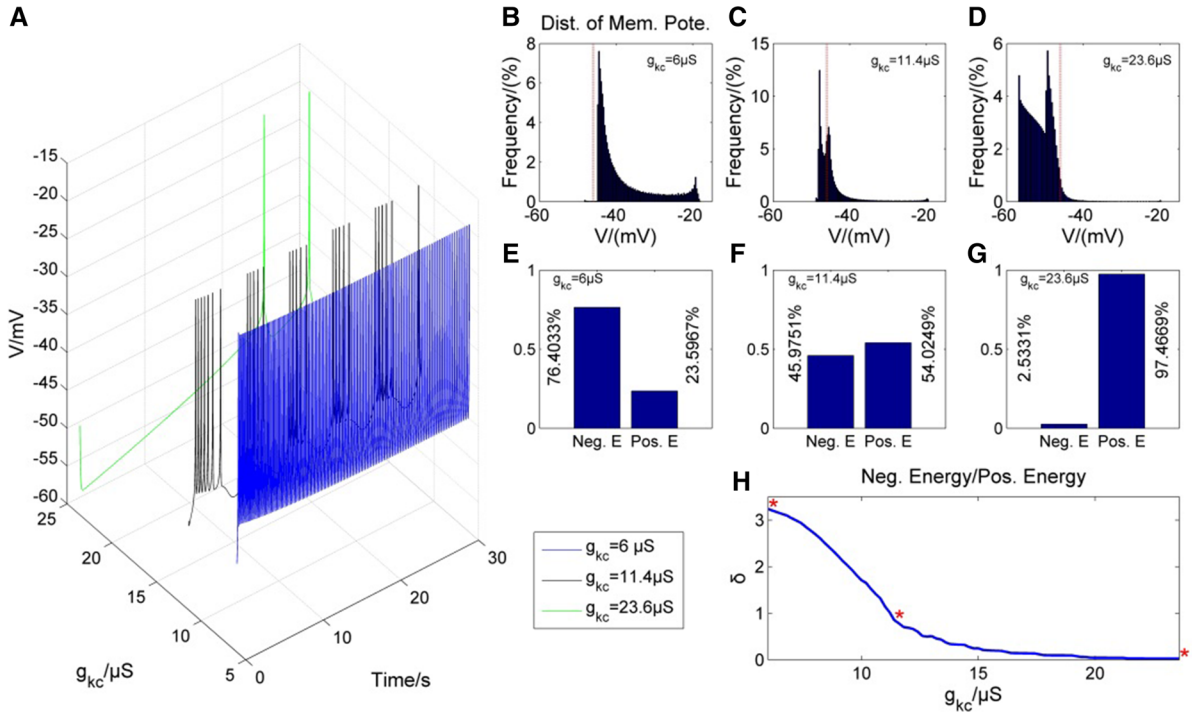

Fig. 4 Negative and positive energy consumption of firing patterns with different firing frequencies and different degrees of hyperpolarization. **a** Three typical firing patterns: high-frequency firing with $g_{kc} = 6\,\mu S$ (the blue line); medium-frequency firing with $g_{kc} = 11.4\,\mu S$ (the black line); low-frequency firing with $g_{kc} = 23.6\,\mu S$ (the green line). **b**, **e** Membrane potential distribution (**b**) and the proportion of negative and positive energy consumption (**e**) in the high-frequency firing pattern with $g_{kc} = 6\,\mu S$. The red dotted line represents the threshold potential of -46 mV. **c**, **f** The membrane potential distribution (**c**) and the proportion of negative and positive energy consumption (**f**) in the medium-frequency firing pattern with $g_{kc} = 11.4\,\mu S$. **d**, **g** The membrane potential distribution (**d**) and the proportion of negative and positive energy consumption (**g**) in the low-frequency firing pattern with $g_{kc} = 23.6\,\mu S$. **h** The ratio of negative energy consumption to positive energy consumption as a function of g_{kc}. The three red stars represent the ratios of the three firing patterns in **a**, respectively. (Color figure online)

regular burst firing pattern, within which each burst is followed by prominent hyperpolarization (Fig. 4c). This medium-frequency pattern consumes relatively balanced negative energy and positive energy (Fig. 4f). At a large value of $g_{kc} = 23.6$ (the green line in Fig. 4a), the membrane potential V is mostly hyperpolarized (between -57 and -46 mV, Fig. 4d), and only two spikes are discharged due to the strong hyperpolarization current I_{kc}. This low-frequency pattern consumes almost exclusively positive energy (more than 97%, Fig. 4g) because hyperpolarization consumes only positive energy (Fig. 2d).

These three patterns, with their contrasting firing properties in terms of the number of spikes and the extent of hyperpolarization, exhibit contrasting $E_n - E_p$ ratios, as marked with red stars in Fig. 4h. The $E_n - E_p$ ratio of high-frequency patterns is much greater than 1 (from 2.224 to 3.238), and that of low-frequency patterns is far less than 1 (from .02599 to 0.6641); however, that of medium-frequency patterns is relatively closer to 1 (non-SBFs: from 1.416 to 2.118; SBFs: from 0.6884 to 1.321). Thus, positive energy and negative energy are consumed in a relatively balanced ratio in producing spikes with hyperpolarization in medium-frequency patterns compared with high- and low-frequency patterns.

To evaluate the energy efficiency of different firing patterns produced by changing g_{kc}, we calculated the carried information CV from Eq. (21) and the energy consumption E from Eq. (18) for each pattern. Figure 5a shows that both high-frequency patterns and medium-frequency patterns carry relatively high amounts of information (the red dotted line), while low-frequency patterns carry low amounts of infor-

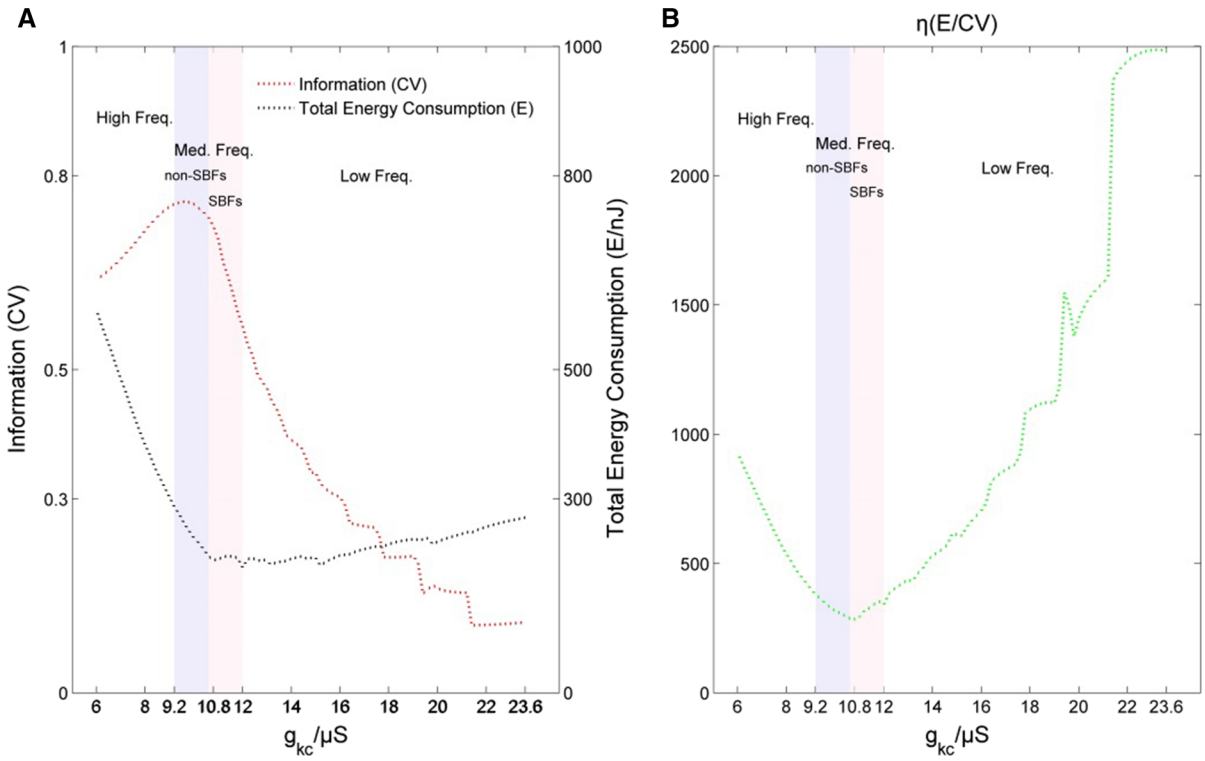

Fig. 5 Energy-efficient sparse burst firing patterns (SBFs) with low energy consumption but a high level of irregularity of information. **a** The carried information CV and neural energy consumption E of all firing patterns arising from changing g_{kc}. **b** The corresponding energy consumption per unit of information η. Both figures are divided into three regions: high-frequency patterns, medium-frequency patterns (distinguished between SBFs and non-SBFs), and low-frequency patterns. (Color figure online)

mation, precisely because the spikes are so rare. The high levels of information carried by high-frequency patterns mainly result from their high firing rates. Both medium-frequency patterns and low-frequency patterns consume relatively low levels of energy (the black dotted line), while high-frequency patterns consume much higher levels of energy due to the large number of spikes. Thus, medium-frequency patterns consume roughly as little energy as low-frequency patterns do, but they can carry nearly as much information as high-frequency patterns (the colored bars in Fig. 5a). As a result, the value η in Eq. (22), i.e., the energy consumed per unit of transmitted information, reaches its minimum in medium-frequency patterns (Fig. 5b), indicating that the energy efficiency of medium-frequency patterns is greater than that of both high- and low-frequency patterns. The maximum energy efficiency (minimum η) is attained by an SBF pattern at $g_{kc} = 10.8$. This optimal SBF pattern has a medium number of total spikes ($N = 34$), a short burst ($N_b = 8$), a low burst probability of about 4%, and a balanced ratio ($\delta = 1.321$) of negative energy to positive energy (Figs. 3, 4h). A comparison between SBF and non-SBF patterns shows that they reach similar levels of energy efficiency (the colored bars in Fig. 5b). Although SBFs carry somewhat less information than non-SBFs do, they clearly consume less energy (the colored bars in Fig. 5a). These results suggest that SBFs may offer advantages over non-SBFs (and all other patterns) in sensory systems since information processing is thought to be under strong selective pressure not only to achieve energy efficiency but also to save energy [20].

To further understand how medium-frequency SBF patterns can carry as much information as high-frequency patterns while consuming as little energy as low-frequency patterns (Fig. 5a), we first examined the relationship between the total energy consumption E

and the $E_n - E_p$ ratio δ in Fig. 6a. The total energy consumed in low-frequency patterns is mostly positive energy with $0.02599 \leqslant \delta \leqslant 0.6641$. This positive energy is consumed in maintaining the membrane potential hyperpolarized (see Fig. 4). By contrast, the SBFs, by making relatively balanced use of positive and negative energy ($0.6884 \leqslant \delta \leqslant 1.321$), are able to produce more spikes while consuming as little total energy as low-frequency patterns. Since the burst size influences the spike-timing structure and carried information, we next determined the information carried by each spike in firing patterns with different burst sizes. As shown in Fig. 6b, short bursts permit much higher information capacity per spike than do long bursts, thus allowing SBFs with short bursts ($3 \leqslant N_b \leqslant 8$) to carry a high level of information even though the total number of spikes is moderate. Although low-frequency patterns with short bursts ($N_b = 2$) have high information capacity per spike, they in fact carry very little information because they fire so few spikes. In a recent study, Naud et al. also found that short and sparse bursts help to maximize the information transferred in multiplexed coding [4]. Therefore, medium-frequency SBFs achieve high energy efficiency because they make balanced use of positive and negative energy and maximize the coded information by combining short bursts and single spikes.

3.2 Energy efficiency of firing patterns resulting from changing the parameter λ_n of the relaxation time constant of voltage-dependent K^+ channels

We next examined how the scaling term λ_n for the relaxation time constant of voltage-dependent K^+ channels in Eq. (14) alone affects the energy efficiency of firing patterns. A change in λ_n (with a fixed g_{kc} of 11) produces different firing patterns (Fig. 7a) by altering how the K^+ current I_k affects the membrane potential V (Fig. 7b). As λ_n increases, the firing patterns shift from medium-frequency tonic firing (the blue line) to sparse burst firing (the black line) and finally to the burst mode of high-frequency spikes (the green line), while the width and amplitude of the spikes progressively decrease. For each firing pattern, we determined the burst size N_b (the red points in Fig. 7c), the number of single spikes N_s (the green points in Fig. 7c), the total number of spikes N, and the probability of bursts. SBFs are generated in a λ_n range from 205 to 240 (the pink bar in Fig. 7c). As shown in Fig. 7d, changes in λ_n alone clearly influence the energy efficiency of firing patterns, and medium-frequency SBF patterns are more energy efficient than other patterns. The energy efficiency of the most efficient SBF pattern resulting from changing λ_n is almost as great as that of the optimal SBF pattern resulting from changing g_{kc} in Fig. 5b.

3.3 Energy efficiency of firing patterns resulting from simultaneous changes in the two parameters g_{kc} and λ_n

We next investigated the energy efficiency of firing patterns generated in an expanded two-dimensional parametric space (g_{kc}, λ_n) to verify the result in Sects. 3.1 and 3.2 SBFs are energy efficient. The simultaneous changes of g_{kc} and λ_n generate SBF patterns in the green area (Fig. 8a), which is outlined in the following figures to highlight various characteristics of SBFs. These SBF patterns discharge a moderate number of spikes (roughly 25 to 50, Fig. 8b), use negative and positive energy in a balanced ratio close to 1 (Fig. 8c), and carry a relatively high level of information (Fig. 8d) while consuming very low levels of total energy (Fig. 8e). Consequently, most SBFs attain high levels of energy efficiency (Fig. 8f). Notably, as shown in Fig. 8f, as λ_n decreases below 220, the SBF patterns become less energy efficient because the amplitude of the APs increases, leading to higher energy consumption (Fig. 8e) without any increase in the information transmitted (Fig. 8d) due to the unchanged number of spikes (Fig. 8b). As it turns out, the firing pattern with the maximum energy efficiency is the same optimal SBF in Sect. 3.1, namely $g_{kc} = 10.8$ and $\lambda_n = 230$ (indicated by the white point in each figure).

Besides these SBFs, other firing patterns also exhibit relatively high energy efficiency (the red, orange, and yellow areas in Fig. 8f). Most of these patterns fire spikes in medium frequencies (Fig. 8b), carry a relatively high level of information (Fig. 8d), and consume relatively low levels of the total energy (Fig. 8e). The energy efficiency of the remaining firing patterns is very low. Their efficiency is primarily determined by g_{kc}, while λ_n has little effect (Fig. 8f). For example, when g_{kc} is very small (6–7), the neuron fires in high-frequency patterns, and its firing rate continuously increases as λ_n increases (Fig. 8b left), resulting in great energy consumption E (Fig. 8e left) and high $E_n - E_p$

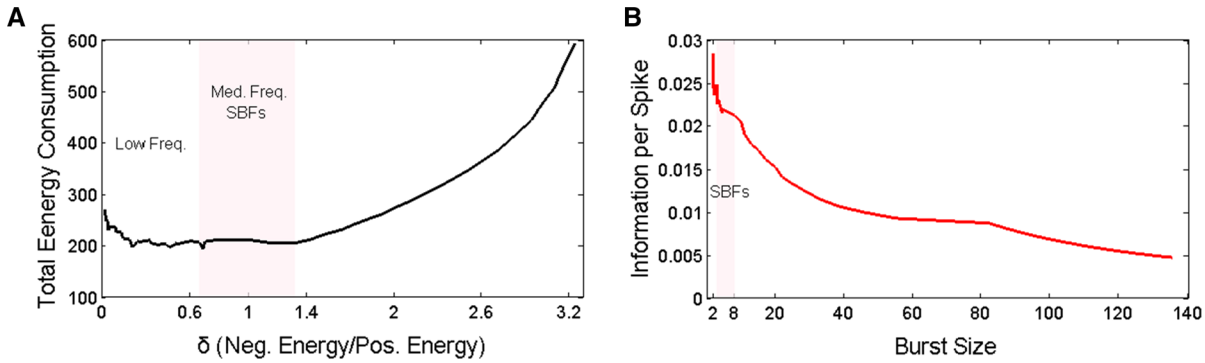

Fig. 6 **a** Total energy consumption as a function of the $E_n - E_p$ ratio δ. **b** The information capacity per spike (CV/spike) decreases as a function of burst size

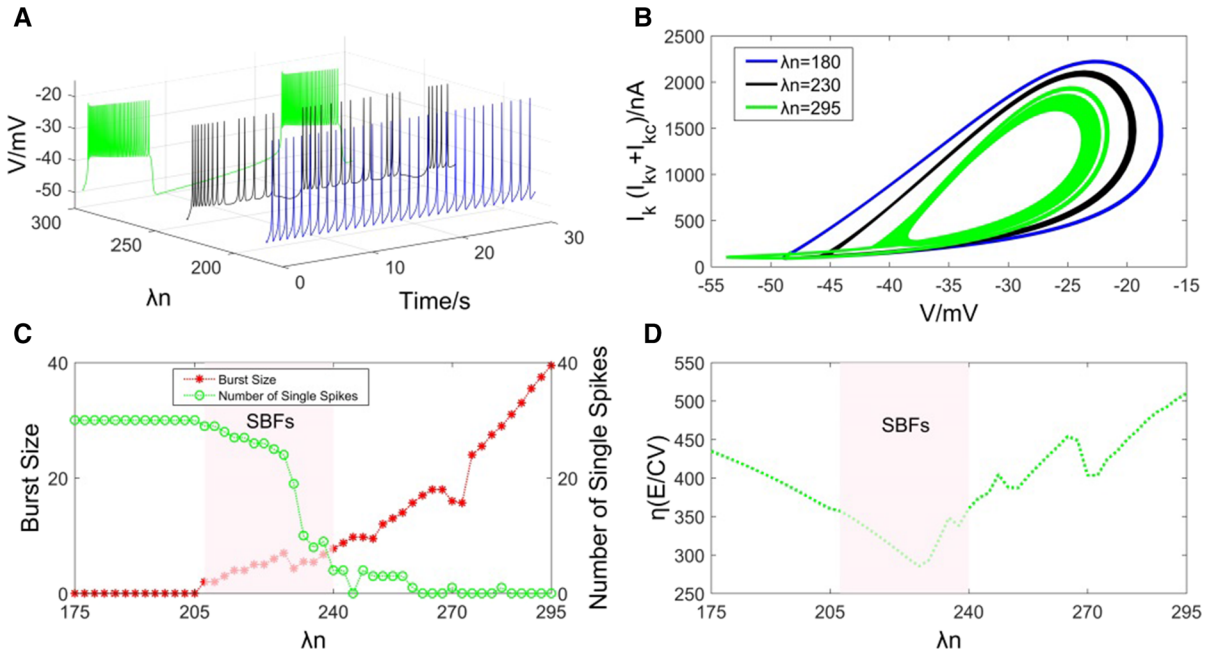

Fig. 7 Energy efficiency of firing patterns arising from changing the relaxation time constant of voltage-dependent K^+ channels λ_n with a fixed g_{kc} of 11. **a** Three typical firing patterns with different λ_n. **b** The corresponding I_k–V curves of these three firing patterns. **c** Burst sizes (the red points) and the number of single spikes (the green points). **d** The energy consumption per unit of information η of all firing patterns of λ_n. (Color figure online)

ratio δ (Fig. 8c left). While these high-frequency patterns can carry nearly the highest levels of information (Fig. 8d left), their energy efficiency is much worse than that of medium-frequency patterns (Fig. 8f left) because of the great energy consumption. When g_{kc} is large (16–23.6), the firing patterns have few spikes ($N < 20$, Fig. 8b right) and consume low levels of energy (Fig. 8e right), most of which are positive energy (Fig. 8c); however, since they carry so little information (Fig. 8d right), their energy efficiency is also quite low (Fig. 8f right).

Therefore, the results obtained by varying the two-dimensional parameters (g_{kc}, λ_n) are consistent with those by changing g_{kc} and λ_n separately. Medium-frequency firing patterns are more energy efficient than high- and low-frequency patterns. The most energy-efficient patterns are predominantly medium-

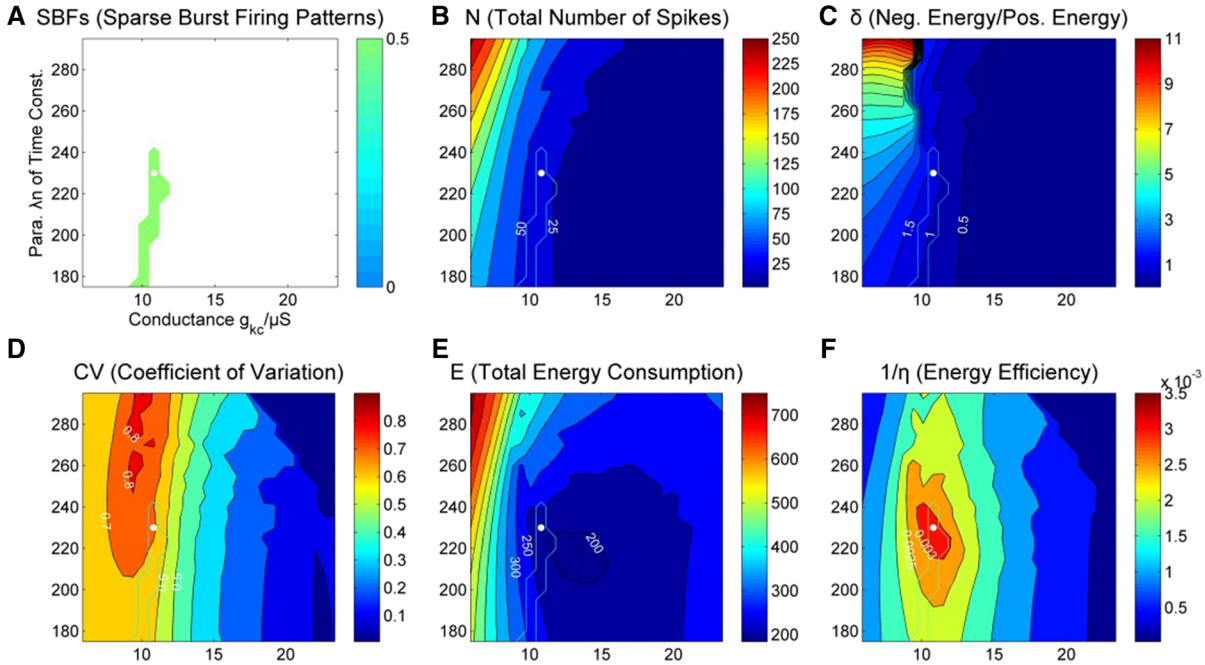

Fig. 8 Energy efficiency of all firing patterns arising from changing g_{kc} and λ_n simultaneously. **a** The green area in which the neuron fires in SBFs. The white point in each figure represents the most efficient firing pattern, which happens to be an SBF. This same area is outlined in the subsequent figures. **b** The total number of spikes N. **c** The ratio δ of negative energy consumption to positive energy consumption. **d** The amount of carried information CV. **e** Neural energy consumption E. **f** Energy efficiency. Note that the color spectrum represents 1/η for the better exhibition of the figure. The red end (large values) and the blue end (small values) of the spectrum represent greater and less energy efficiency, respectively. In all figures, the horizontal and vertical axes represent the maximal conductance of the Ca^{2+}-dependent K^+ channel g_{kc} and the relaxation time constant of voltage-dependent K^+ channel λ_n, respectively. The ranges of g_{kc} (6–23.6) and λ_n (175–295) are chosen to focus on firing patterns commonly observed in the sensory system. (Color figure online)

frequency SBFs generated by modulating both calcium-dependent and voltage-dependent K^+ currents.

Finally, we examined the effect of the duration T on the energy efficiency of firing patterns. T, which was previously set at 30 s, is now varied from 5 to 60 s at intervals of 5 s. For each T, we calculated the most energy-efficient pattern among all tested firing patterns of g_{kc}-λ_n pairs. At $T>5$ s, the most energy-efficient patterns are all SBFs because their burst size N_b is about 6–8 spikes and burst probability is less than 35%; at $T = 5$ s, none of the g_{kc}–λ_n pairs produce an SBF pattern. In addition, the $E_n - E_p$ ratios of these most energy-efficient firing patterns are around 1.3. These results suggest that the variation of T has no significant effect on the results in this study.

4 Discussion

Our findings indicate that SBF patterns in medium frequencies are more energy efficient than high-frequency patterns with massive spikes and low-frequency patterns with rare spikes. This greater energy efficiency is caused by two key factors. First, energy consumption is reduced by limiting the number of spikes to medium levels and by a balanced use of negative and positive energy. Second, with fewer spikes, the combination of burst and single-spike modes helps to increase the temporal variability of spike trains and thus the information carried by SBFs. Although high-frequency patterns can carry somewhat more information by discharging a large number of spikes, these spikes are very costly in terms of energy consumption, therefore leading to less energy efficiency. Low-frequency patterns conserve energy by keeping the membrane potential

hyperpolarized, thus limiting the number of energy-costly spikes. These few spikes, however, carry very little information, resulting in even worse energy efficiency.

The energy consumption that contributes to membrane potential changes during a firing pattern is influenced by both the number of spikes N and the ratio of negative to positive energy consumption of this pattern, but in different ways. For high-frequency patterns, energy consumption is positively correlated to N with a Pearson correlation coefficient of nearly 1. Therefore, the energy consumption of high-frequency patterns is basically determined by N. When a neuron fires a moderate or small number of spikes, the energy consumption remains low but does not decline with the decreasing number of firing spikes. Instead, the energy consumption is influenced by the $E_n - E_p$ ratio of the firing pattern. In low-frequency patterns, the neuron consumes energy to keep the membrane potential hyperpolarized so as to limit the number of energy-costly spikes. In contrast, in medium-frequency SBFs, a balanced use of negative energy and positive energy helps to lower the total energy consumption below that of low-frequency patterns while firing a moderate number of spikes transmits more information and thus improves the energy efficiency. From the view of energy consumption, this may also explain why neurons in sensory systems frequently fire spikes spontaneously rather than remain in resting or hyperpolarized membrane potential [50], as both activities likely consume similar amounts of energy. Based on our results, the most efficient SBF consumes these two kinds of energy in an optimal way, with an $E_n - E_p$ ratio of 1.321.

In fact, during a firing pattern in time period T, the actual energy amounts consumed from the Na^+ concentration gradient and the K^+ concentration gradient are $\int_0^T |I_i V_i| \, dt$ and $\int_0^T |I_k V_k| \, dt$, respectively; the former is almost exclusively derived from the Na^+ concentration gradient because the concentration gradient of Ca^{2+} is indeed mostly maintained by Na^+–Ca^{2+} exchangers, which use the concentration gradient of Na^+ to transport Ca^{2+} out of the neuron [38,51]. For the most energy-efficient SBF, this ratio of $\int_0^T |I_i V_i| \, dt \Big/ \int_0^T |I_k V_k| \, dt$ is 1.165, which is close to the ratio 3:2 at which Na/K-ATPase pumps work for Na^+ and K^+ ionic concentration gradients. As we know, Na/K-ATPase pumps actively extrude three Na^+ and import two K^+ for the hydrolysis of one ATP to store potential energy in the form of ionic gradients of both Na^+ and K^+ [38,51]. The fact that this ratio of using the concentration gradients of Na^+ and K^+ is lower than 3:2 can be explained by the following mechanism. Unlike the stored K^+ concentration gradient, the stored Na^+ concentration gradient is used not only to provide energy for membrane potential changes but also to move other ions or neurotransmitters, such as H^+ and GaBa dopamine, up their concentration gradients [38]. Thus, it is likely that the most energy-efficient firing pattern makes full use of the concentration gradients of Na^+ and K^+ in a ratio close to but somewhat less than 3:2. For SBF patterns in general, this ratio is close to 1 (from 1.047 to 1.165). Therefore, SBFs, which consume negative energy and positive energy in a balanced way, are actually making relatively full use of the stored energy created by Na/K-ATPase pumps. In fact, firing spikes alone without hyperpolarization consumes more of the Na^+concentration gradient, while hyperpolarization consumes only the K^+concentration gradient. Hence, the timing structure of SBF patterns—the hyperpolarization process that follows a short burst of spikes—helps to balance the use of Na^+ and K^+concentration gradients.

In contrast, high-frequency patterns make excessive use of the potential energy stored in the Na^+ concentration gradient without fully using the energy stored in the K^+ concentration gradient. This unbalanced usage of ion concentration gradients may result in inefficient use of energy stored in the neuron. The redundant K^+ concentration gradient may be passively released at rest through leakage K^+ channels [38] without inducing a change in the membrane potential, resulting in a waste of energy. However, such high-frequency patterns are commonly observed in fast-spiking interneurons in sensory systems, suggesting that the evolutionary pressure for these neurons may be to propagate spikes rapidly rather than give priority to save energy to increase energy efficiency [22,24]. Low-frequency patterns, on the other hand, under-consume energy stored in the Na^+ concentration gradient and over-consume energy stored in the K^+gradient. The redundant Na^+ concentration gradient may spontaneously induce sparse spikes [51], also leading to a waste of energy in terms of information transmission.

Our study measured carried information in terms of the variability of spike trains. Information is weakly correlated to the number of firing spikes in high-frequency firing patterns. It is more efficient to pro-

duce informative spikes through a mix of short bursts and single spikes to augment the amount of transmitted information. The findings are in line with those in the study by Naud et al. [4], in which sparse bursts help to maximize the information transferred in multiplexed coding. In reality, however, the coding of information is likely to be more complex [11–14,52]. Indeed, a recent study argues that high-frequency bursts and low-frequency single spikes in the same spike train can encode different types of information, and burst modes may carry much more information than previously thought [53]. Further study on the information carried in bursts and single spikes is needed to evaluate the efficiency of different firing patterns.

Nevertheless, our results do support the experimental findings of Laughlin et al., that "the minimization of the metabolic cost promotes the distribution of signals over a population of weakly active cells" [16]. We extrapolate from the relationship between carried information and energy consumption (Fig. 5a) that in a multi-neuron system, two or more neurons firing in SBF patterns are able to transmit significantly more information than does a single neuron firing high-frequency spikes when they consume the same amount of energy. Thus, in terms of energy efficiency, it is preferable for the sensory system to use multiple neurons to do the work of a single neuron operating at high energy intensity. Indeed, in sensory systems, medium-frequency SBF patterns are very common [1–6,54]. This prevalence of SBFs thus supports the view that in the trade-off between maximizing carried information and minimizing energy consumption, the sensory system gives priority to limiting energy costs over maximizing information in order to achieve greater energy efficiency [16,20,55].

In this study, we examined the energy efficiency of different neural firing patterns simulated with the Chay neuron model. We concluded that medium-frequency SBFs are more energy efficient than other firing patterns. Although our findings are consistent with those in previous studies [4,16], we are aware that these results can be based on the limited number of firing patterns simulated by the Chay model. Other firing patterns simulated by alternative neural models [56–58] should be studied in order to substantiate our findings. It will be also useful to explore the neural energy utilization of different firing patterns at the level of the neural network to gain a better understanding of the encoding mechanism of neural information processing under energy limitation [52,59–62].

Acknowledgements This work was supported by the National Natural Science Foundation of China (Grants Nos. 11232005, 11472104, 11872180, and 11972159) and the China Scholarship Council (CSC No. 201706740042). This manuscript was communicated by Professor Wang Rubin at rbwang@163.com during the submission and revision.

Compliance with ethical standards

Conflict of interest The authors declare that they have no conflict of interest.

References

1. Krahe, R., Gabbiani, F.: Burst firing in sensory systems. Nat. Rev. Neurosci. **5**, 13–23 (2004)
2. Bingmer, M., Schiemann, J., Roeper, J., Schneider, G.: Measuring burstiness and regularity in oscillatory spike trains. J. Neurosci. Meth. **201**(2), 426–437 (2011)
3. Bittner, K.C., Grienberger, C., Vaidya, S.P., Milstein, A.D., et al.: Conjunctive input processing drives feature selectivity in hippocampal CA1 neurons. Nat. Neurosci. **18**, 1133–1142 (2015)
4. Naud, R., Sprekeler, H.: Sparse bursts optimize information transmission in a multiplexed neural code. Proc. Natl. Acad. Sci. **115**(27), E6329–E6338 (2018)
5. Martinez-Conde, S., Macknik, S.L., Hubel, D.H.: The function of bursts of spikes during visual fixation in the awake primate lateral geniculate nucleus and primary visual cortex. Proc. Natl. Acad. Sci. **99**(21), 13920–13925 (2002)
6. Snider, R.K., Kabara, J.F., Roig, B.R., Bonds, A.B.: Burst firing and modulation of functional connectivity in cat striate cortex. J. Neurophysiol. **80**, 730–744 (1998)
7. Cardin, J.A., Carlén, M., Meletis, K., Knoblich, U., et al.: Driving fast-spiking cells induces gamma rhythm and controls sensory responses. Nature **459**, 663–667 (2009)
8. Schiemann, J., Schlaudraff, F., Klose, V., Bingmer, M., et al.: K-ATP channels in dopamine substantia nigra neurons control bursting and novelty-induced exploration. Nat. Neurosci. **15**, 1272–1280 (2012)
9. Mondal, A., Upadhyay, R.K., Ma, J., Yadav, B.K., et al.: Bifurcation analysis and diverse firing activities of a modified excitable neuron model. Cogn. Neurodyn. **13**, 393–407 (2019)
10. Goldberg, J.A., Wilson, C.J.: Control of spontaneous firing patterns by the selective coupling of calcium currents to calcium-activated potassium currents in striatal cholinergic interneurons. J. Neurosci. **25**(44), 10230–10238 (2005)
11. Berry, M.J., Warland, D.K., Meister, M.: The structure and precision of retinal spike trains. Proc. Natl. Acad. Sci. **94**(10), 5411–5416 (1997)
12. Strong, S.P., Koberle, R., de Ruyter van Steveninck, R.R., Bialek, W.: Entropy and information in neural spike trains. Phys. Rev. Lett. **80**, 197 (1998)

13. Masuda, N., Aihara, K.: Bridging rate coding and temporal spike coding by effect of noise. Phys. Rev. Lett. **88**, 248101 (2002)
14. Zhu, J., Liu, X.: Measuring spike timing distance in the Hindmarsh–Rose neurons. Cogn. Neurodyn. **12**, 225–234 (2018)
15. Malagarriga, D., Pons, A.J., Villa, A.E.P.: Complex temporal patterns processing by a neural mass model of a cortical column. Cogn. Neurodyn. **13**, 379–392 (2019)
16. Laughlin, S.B., de Ruyter van Steveninck, R.R., Anderson, J.C.: The metabolic cost of neural information. Nat. Neurosci. **1**, 36–41 (1998)
17. Zheng, H., Wang, R., Qiao, L., Du, Y.: The molecular dynamics of neural metabolism during the action potential. Sci. China Technol. Sci. **57**, 857–863 (2014)
18. Wang, Y., Wang, R., Xu, X.: Neural energy supply-consumption properties based on Hodgkin–Huxley model. Neural Plast. **2017**, 6207141 (2017)
19. Sengupta, B., Stemmler, M., Laughlin, S.B., Niven, J.E.: Action potential energy efficiency varies among neuron types in vertebrates and invertebrates. PLoS Comput. Biol. **6**(7), e1000840 (2010)
20. Laughlin, S.B.: Energy as a constraint on the coding and processing of sensory information. Curr. Opin. Neurobiol. **11**(4), 475–480 (2001)
21. Alle, H., Roth, A., Geiger, J.R.P.: Energy-efficient action potentials in hippocampal mossy fibers. Science **325**(5946), 1405–1408 (2009)
22. Carter, B.C., Bean, B.P.: Sodium entry during action potentials of mammalian neurons: incomplete inactivation and reduced metabolic efficiency in fast-spiking neurons. Neuron **64**(6), 898–909 (2009)
23. Sengupta, B., Laughlin, S.B., Niven, J.E.: Balanced excitatory and inhibitory synaptic currents promote efficient coding and metabolic efficiency. PLoS Comput. Biol. **9**, e1003263 (2013)
24. Moujahid, A., d'Anjou, A.: Metabolic efficiency with fast spiking in the squid axon. Front. Comput. Neurosci. **6**, 95 (2012)
25. Brown, M.R., Kaczmarek, L.K.: Potassium channel modulation and auditory processing. Hear. Res. **279**(1–2), 32–42 (2011)
26. Meng, X., Lu, Q., Rinzel, J.: Control of firing patterns by two transient potassium currents: leading spike, latency, bistability. J. Comput. Neurosci. **31**, 117–136 (2011)
27. Johnston, J., Forsythe, I.D., Kopp-Scheinpflug, C.: Going native: voltage-gated potassium channels controlling neuronal excitability. J. Physiol. **588**, 3187–3200 (2010)
28. Ma, J., Yang, Z., Yang, L., Tang, J.: A physical view of computational neurodynamics. J. Zhejiang Univ. Sci. A **20**, 639–659 (2019)
29. Wang, R., Zhu, Y.: Can the activities of the large scale cortical network be expressed by neural energy? A brief review. Cogn. Neurodyn. **10**, 1–5 (2016)
30. Kriegeskorte, N., Douglas, P.K.: Cognitive computational neuroscience. Nat. Neurosci. **21**, 1148–1160 (2018)
31. Kass, R.E., Amari, S., Arai, K., Brown, E.N., et al.: Computational neuroscience: mathematical and statistical perspectives. Annu. Rev. Stat. Appl. **5**, 183–214 (2018)
32. Chay, T.R.: Chaos in a three-variable model of an excitable cell. Physica D **16**(2), 233–242 (1985)
33. Li, L., Gu, H., Yang, M., Liu, Z., Ren, W.: A series of bifurcation scenarios in the firing pattern transitions in an experimental neural pacemaker. Int. J. Bifurc. Chaos **14**(5), 1813–1817 (2004)
34. Ando, H., Suetani, H., Kurths, J., Aihara, K.: Chaotic phase synchronization in bursting-neuron models driven by a weak periodic force. Phys. Rev. E **86**, 016205 (2012)
35. Jia, B., Gu, H., Xue, L.: A basic bifurcation structure from bursting to spiking of injured nerve fibers in a two-dimensional parameter space. Cogn. Neurodyn. **11**, 189–200 (2017)
36. Wang, R., Wang, Z., Zhu, Z.: The essence of neuronal activity from the consistency of two different neuron models. Nonlinear Dyn. **92**, 973–982 (2018)
37. Zhu, F., Wang, R., Pan, X., Zhu, Z.: Energy expenditure computation of a single bursting neuron. Cogn. Neurodyn. **13**, 75–87 (2019)
38. Kandel, E.R., Schwartz, J.H., Jessell, T.M., Siegelbaum, S.A., Hudspeth, A.J.: Principles of Neural Science, 5th edn. McGraw-Hill Companies, New York (2013)
39. Moujahid, A., d'Anjou, A., Torrealdea, F.J., Torrealdea, F.: Energy and information in Hodgkin–Huxley neurons. Phys. Rev. E **83**, 031912 (2011)
40. Wang, R., Tsuda, I., Zhang, Z.: A new work mechanism on neuronal activity. Int. J. Neural Syst. **25**(3), 1450037 (2015)
41. Wang, Y., Wang, R.: An improved neuronal energy model that better captures of dynamic property of neuronal activity. Nonlinear Dyn. **91**, 319–327 (2018)
42. Levy, W.B., Baxter, R.A.: Energy efficient neural codes. Neural Comput. **8**(3), 531–543 (1996)
43. Tozzi, A., Peters, J.F., Çankaya, M.N.: The informational entropy endowed in cortical oscillations. Cogn. Neurodyn. **12**, 501–507 (2018)
44. de Ruyter van Steveninck, R.R., Lewen, G.D., Strong, S.P., Koberle, R., Bialek, W.: Reproducibility and variability in neural spike trains. Science **275**(5307), 1805–1808 (1997)
45. Sadeghi, S.G., Chacron, M.J., Taylor, M.C., Cullen, K.E.: Neural variability, detection thresholds, and information transmission in the vestibular system. J. Neurosci. **27**(4), 771–781 (2007)
46. Nawrot, M.P., Boucsein, C., Molina, V.R., Riehle, A., et al.: Measurement of variability dynamics in cortical spike trains. J. Neurosci. Methods **169**(2), 374–390 (2008)
47. Shadlen, M.N., Newsome, W.T.: The variable discharge of cortical neurons: implications for connectivity, computation, and information coding. J. Neurosci. **18**(10), 3870–3896 (1998)
48. Harmony, T.: The functional significance of delta oscillations in cognitive processing. Front. Integr. Neurosci. **7**, 83 (2013)
49. Kopell, N., Ermentrout, G.B., Whittington, M.A., Traub, R.D.: Gamma rhythms and beta rhythms have different synchronization properties. Proc. Natl. Acad. Sci. **97**(4), 1867–1872 (2000)
50. Fox, M.D., Raichle, M.E.: Spontaneous fluctuations in brain activity observed with functional magnetic resonance imaging. Nat. Rev. Neurosci. **8**, 700–711 (2007)
51. Koch, C.: Biophysics of Computation. Oxford University Press, Oxford (1999)

52. Mateos, D.M., Guevara Erra, R., Wennberg, R., et al.: Measures of entropy and complexity in altered states of consciousness. Cogn. Neurodyn. **12**, 73–84 (2018)
53. Mease, R.A., Kuner, T., Fairhall, A.L., Groh, A.: Multiplexed spike coding and adaptation in the thalamus. Cell Rep. **19**(6), 1130–1140 (2017)
54. Wang, G., Wang, R., Kong, W., Zhang, J.: Simulation of retinal ganglion cell response using fast independent component analysis. Cogn. Neurodyn. **12**, 615–624 (2018)
55. Wolfe, J., Houweling, A.R., Brecht, M.: Sparse and powerful cortical spikes. Curr. Opin. Neurobiol. **20**(3), 306–312 (2010)
56. Yao, Z., Ma, J., Yao, Y., Wang, C.: Synchronization realization between two nonlinear circuits via an induction coil coupling. Nonlinear Dyn. **96**, 205–217 (2019)
57. Xu, Y., Ma, J., Zhan, X., Yang, L., Jia, Y.: Temperature effect on memristive ion channels. Cogn. Neurodyn. **13**, 601–611 (2019)
58. Ma, J., Zhang, G., Hayat, T., Ren, G.: Model electrical activity of neuron under electric field. Nonlinear Dyn. **95**, 1585–1598 (2019)
59. Zhu, Z., Wang, R., Zhu, F.: The energy coding of a structural neural network based on the Hodgkin–Huxley model. Front. Neurosci. **12**, 122 (2018)
60. Lu, L., Jia, Y., Kirunda, J.B., Xu, Y., et al.: Effects of noise and synaptic weight on propagation of subthreshold excitatory postsynaptic current signal in a feed-forward neural network. Nonlinear Dyn. **95**, 1673–1686 (2019)
61. Xu, Y., Jia, Y., Wang, H., Liu, Y., et al.: Spiking activities in chain neural network driven by channel noise with field coupling. Nonlinear Dyn. **95**, 3237–3247 (2019)
62. Ge, M., Jia, Y., Lu, L., Xu, Y., et al.: Propagation characteristics of weak signal in feedforward Izhikevich neural networks. Nonlinear Dyn. **99**, 2355–2367 (2020)

Publisher's Note Springer Nature remains neutral with regard to jurisdictional claims in published maps and institutional affiliations.